Targeted Search for Fast Radio Bursts with Nanshan 26 m Radio Telescope

Jian-Wei Mao[1,2], Jian-Ping Yuan[1], Zhi-Gang Wen[1], Jian Li[1], Na Wang[1], Pei Wang[3], Rai Yuen[1], Yu-Bin Wang[1,2] (ORCID),
Nan-Nan Zhai[1,2], Zhi-Yong Liu[1], Mao-Zheng Chen[1], and Guang-Hui Li[1]

[1] Xinjiang Astronomical Observatory, Chinese Academy of Sciences, Urumqi, Xinjiang 830011, China; yuanjp@xao.ac.cn
[2] University of Chinese Academy of Sciences, Beijing 100049, China
[3] National Astronomical Observatories, Chinese Academy of Sciences, Beijing 100101, China

Abstract

Fast radio bursts (FRBs) are radio transients that are bright and have short duration, with their physical mechanism not being fully understood. We conducted a targeted search for bursts from FRB 20201124A between 2021 June 2 and July 20. High time-resolution data were collected for 104.5 hr using the ROACH2-based digital backend. We introduce the details of our FRB search pipeline which is based on HEIMDALL and FETCH. Testing of the injected mock FRBs search could help us better understand the performance of the pipelines, and improve the search algorithms and classifiers. To study the efficiency of our pipeline, 5000 mock FRBs were injected into the data and searched using the pipeline. The results of the mock FRB search show that our pipeline can recover almost all ($\gtrsim$90%) the injected mock FRBs above a signal-to-noise ratio (S/N) threshold of 15, and the performance is still acceptable ($\gtrsim$80%) for injected S/Ns from 10 to 15. The recovery fraction displays relations with S/N, dispersion measure and pulse width. No bursts were detected from FRB 20201124A in the middle of 2021. The non-detection of FRB 20201124A may be due to its quiet phase window or no emission above the threshold of the Nanshan telescope.

Key words: transients: fast radio bursts – methods: observational – methods: data analysis

1. Introduction

Fast radio bursts (FRBs) are radio bursts that are bright and have short duration, with their physical mechanism not being fully understood. The first FRB was found by Lorimer et al. (2007) in the archival data of the Parkes telescope. Up to now, several hundred FRB sources have been detected with most being one-off events but dozens of sources are repeating such as FRB 20121102 (Spitler et al. 2016). Most FRBs have high dispersion measures (DMs) along their line-of-sight directions, which are usually larger than the DM provided by the Galaxy, suggesting a likely extragalactic origin. Most repeating FRBs, which were discovered by the Canadian Hydrogen Intensity Mapping Experiment (CHIME), are included in the catalog of 536 FRBs (CHIME/FRB Collaboration et al. 2021a). Among all the repeating FRBs, FRB 180916.J0158+65 was identified with a burst activity period of 16.35 days (CHIME/FRB Collaboration et al. 2020). An extremely strong radio burst was detected at 1.4 GHz from the Galactic magnetar SGR 1935 +2154. The burst fluence was 1.5 MJy ms indicating that some FRBs probably originated from magnetar activities (Bochenek et al. 2020). Some FRBs are claimed to have sub-second periodicity in multi-component pulse profiles. For example, pulse profiles of FRB 20210206A and FRB 20210213A exhibit some signs of periodic separations of 2.8(1) and 10.7(1) ms, respectively (The CHIME/FRB Collaboration et al. 2021).

FRB 20201124A (DM $\approx$ 410 pc cm^{-3}) is a bright and energetic repeating source discovered by CHIME, which entered an active period in April 2021 (CHIME/FRB Collaboration et al. 2021b). In April and May 2021, thousands of bursts were detected from 400 MHz to 1.5 GHz, and the bursts exhibit band limited emission (Farah et al. 2021; Herrmann 2021; Hilmarsson et al. 2021; Kirsten et al. 2021; Kumar et al. 2021a, 2021b, 2022; Xu et al. 2021b, 2021a; Marthi et al. 2022). Up to now, no bursts at frequencies higher than 3 GHz have been detected, nor has prompt optical and X-ray emission been confirmed at the time of the bursts (Campana 2021; Zhirkov et al. 2021; Kumar et al. 2022). The bursts of FRB 20201124A feature rich spectral structure, and the average pulse width is wider than other repeating FRBs (Marthi et al. 2022). The bursts of FRB 20201124A also show variable Faraday rotation, and some bursts display highly circularly polarized radiation, indicating that the source is in a complex magnetic environment (Xu et al. 2021b; Kumar et al. 2022).

Many FRB search pipelines are designed to hunt FRBs. Patel et al. (2018) presented a single pulse search pipeline for the Pulsar Arecibo *L*-band Feed Array (PALFA) survey based on PRESTO.[4] Keane et al. (2018) described a real-time search pipeline for both pulsars and FRBs used in the SUrvey for

---

[4] https://github.com/scottransom/presto

Pulsars and Extragalactic Radio Bursts (SUPERB). Taking advantage of the large field of view of the 20-meter telescope, a real-time search system was designed to find FRBs using the 20 m radio dish at the Green Bank Observatory (Golpayegani et al. 2019). Canadian Hydrogen Intensity Mapping Experiment Fast Radio Burst Project (CHIME/FRB), Upgraded Molonglo Observatory Synthesis Telescope (UTMOST) and Robert C. Byrd Green Bank Telescope (GBT) have also designed a real-time FRB search system (CHIME/FRB Collaboration et al. 2018; Farah et al. 2019; Agarwal et al. 2020b). A new FRB was discovered by the Five-hundred-meter Aperture Spherical radio Telescope (FAST) using its artificial intelligence (AI) pipeline (Zhu et al. 2020). Niu et al. (2021) reported the HEIMDALL-based pipeline for Commensal Radio Astronomy FAST Survey (CRAFTS) FRB search, and the discovery of three new FRBs. Recently, a GPU-based single-pulse search pipeline (GSP) has been developed and applied to CRAFTS to accelerate the search (You et al. 2021). A real-time search system called Burst Emission Automatic Roger (BEAR) was designed and implemented at the Nanshan 26 m and Kunming 40 m radio telescopes (Men et al. 2019).

In this paper, we present the details for our off-line FRB search pipeline using the Nanshan 26 m radio telescope (NSRT-26 m) at 1.5 GHz. The paper is organized as follows. In Section 2, we describe our search pipeline and the procedures for radio frequency interference (RFI) mitigation. The test results based on mock FRBs and the real observation data from a bright rotating radio transient (RRAT) source are explored in Section 3. Preliminary search results for FRB 20201124A are demonstrated in Section 4. A summary and discussion of the future work for searching FRBs are presented in Section 5.

2. Observations and Search Pipeline

2.1. Observations

The NSRT-26 m is located at E87°10′.67, N43°28′.27 at an altitude of 2080 m, and is operated by Xinjiang Astronomical Observatory (XAO), Chinese Academy of Sciences (Wang et al. 2001). The receiver for FRB search is centered at 1556 MHz, with bandwidth of 320 MHz, system temperature of 25 K and telescope gain of 0.1 K Jy^{-1}. Using the radiometer equation (Golpayegani et al. 2019)

$$\mathcal{F}_{min} = \frac{T_{sys} S/N}{G} \sqrt{\frac{W}{n_p B}}, \tag{1}$$

the estimated minimum detectable fluence based on a signal-to-noise ratio (S/N) threshold of 10, pulse width of 1 ms and effective bandwidth of 200 MHz after removing the bad frequency channels is about 4 Jy ms. Here, $\mathcal{F}_{min}$ is the minimum detectable fluence; S/N is the pulse S/N; T_{sys} is the system temperature at the observing frequency; G is the

telescope gain; W is the pulse width; n_p is the number of polarizations and B is the observing bandwidth.

The NSRT-26 m observed FRB 20201124A with pointing at R.A. (J2000) = 05^{h}08^{m}03^s.5 and decl. (J2000) = +26°03′37″.8 (Law et al. 2021). A total exposure time of 104.5 hr was accomplished between 2021 June 2 and July 20. The details of the observation dates and durations are shown in Figure 1. We used the analog-to-digital converter (ADC) ADC1x5000-8 and ROACH2[5] hardware platform for data acquisition. The ROACH2 has eight 10 Gb SFP+ Ethernet ports for data transmission and one 1Gb network port for system control. The signal from the receiver is quantized in the ADC which is connected with ROACH2 via two ZDOCK interfaces. The Field Programmable Gate Array (FPGA) programming is implemented by employing the Collaboration for Astronomy Signal Processing and Electronics Research (CASPER[6]) tools. In total, 1024 channels are formed by applying a polyphase filter bank. Then cross-correlation and auto-correlation were computed to obtain full polarization in the format of AABBCRCI, followed by gain adjustment. Data flow with time resolution of 64 μs and 8-bit quantification is packetized and transferred to the recording server via the 10Gb network interface for further processing.

2.2. Overview of Pipeline

Like many other FRB search pipelines, we choose HEIMDALL[7] and FETCH[8] as our searching and classification software. Gupta et al. (2021) have already shown that the root mean square (rms) of a time series with RFI after boxcar convolution will be overestimated, resulting in the reduction of the S/N and width. Therefore, we modified the S/N estimation method inside HEIMDALL, using the rms of time series scaled by the square root of the boxcar width before convolution. FETCH is an open-source package that adopts frequency–time (F–T) and DM–time (D–T) images to classify FRBs and RFI using certain convolution-based neural network models (Agarwal et al. 2020a).

Figure 2 illustrates the schematic of our FRB search pipeline. First, the observed data collected by the telescope are transported from the observation server to the data storage server. Then the raw data, stored in 8-bit PSRFITS format, are converted to filterbank format by summing AA and BB. After mitigating the RFI, we use HEIMDALL to search for the bursts within a certain DM range. The DM-tolerance, which is a configurable tolerance for maximum loss in S/N, is set to 1.2 with the maximum boxcar of 512. The search range of corresponding pulse width is 0.064–32.768 ms, and the S/N threshold is set to 6 for known sources and 10 for unknown

---

5 https://casper.astro.berkeley.edu/wiki/ROACH2
6 https://casper.astro.berkeley.edu/
7 https://sourceforge.net/p/heimdall-astro/wiki/Home/
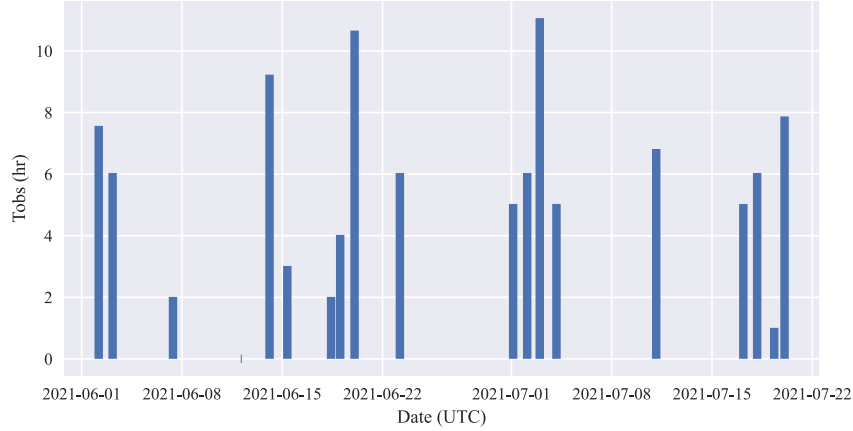8 https://github.com/devanshkv/fetch

Figure 1. Dates and durations of observations for FRB 20201124A with NSRT-26 m.

sources. We use both the a and b models of FETCH to classify the large number of candidates. Model a is a combination of pre-trained DenseNet121 and Xception, and model b uses pre-trained DenseNet121 and VGG16 models (Agarwal et al. 2020a). Finally, the positive candidates are visually inspected by human eyes. The data are processed on the cluster server, which is named Taurus XAO HPC Cluster (Zhang & Nie 2016) and composed of a head node and 16 Compute Nodes with a GPU Nvidia Tesla K20m.

2.3. RFI Mitigation on Data

RFI in the data will lead to a large number of false positive detections and some single pulses missing. The following steps are applied to excise RFI. We apply zero-DM filtering to remove broadband RFI (Eatough et al. 2009), followed by zapping the frequency channels that are always affected by RFI and overpowered. Finally, the samples with more than 6σ of zero-DM time series are replaced by the mean of the frequency channels. Zero-DM filtering calculates the mean of all frequency channels in each time sample and subtracts this from each individual frequency channel in the time sample. However, outliers in the samples, such as narrow-band transient RFI, can easily lead to overestimation of the mean. If the overestimated mean value is subtracted, the baseline of the time series will dip during the process of dedispersion and the amplitude of the signal will be reduced due to baseline dip. This results in a decrease of S/N for a non-optimized matched boxcar filter which is used by most FRBs searching software. Candidate images, such as the F–T and D–T images used by FETCH, will also change due to zero-DM filtering, which may reduce the accuracy of the AI models that are not trained on such samples. In order to reduce the impact on the pulses, we employ the median for the subtraction instead of the mean. For

a complex RFI environment, more careful RFI mitigation on data will be carried out in the future.

3. Pipeline Testing

3.1. Mock FRB Injections

Mock FRB injection is a common and end-to-end approach to test the performance of complete FRB search pipelines. In order to obtain the sensitivity of their pipeline for the PALFA survey, simulated FRBs with certain fixed parameters were inserted into the data and searched for using the pipeline (Patel et al. 2018). Results of the injection test on simulated pulses with different parameters show that almost all inserted pulses with an S/N of more than 12 can be well recovered by their pipeline (Agarwal et al. 2020b). V-FASTR (Wayth et al. 2011), CHIME/FRB (CHIME/FRB Collaboration et al. 2018) and REALFAST (Law et al. 2018) each have a mock FRB injection system to estimate the sensitivity of the pipeline. UTMOST also has an injection system for estimating the efficiency of detection, which shows a ninety percent recovery for about 2000 injection mock FRBs (Farah et al. 2019). Gupta et al. (2021) performed a more comprehensive analysis of the insertion system of UTMOST by inserting 20,000 mock FRBs into the data with uniformly distributed parameters, and analyzed the results obtained from HEIMDALL and Random Forest Classifier.

In order to determine the efficiencies of our FRB search pipeline, we simulated 5000 fake FRBs and injected them into certain PSRFITS data selected from five observation days. The fake FRBs were injected into the data at every 10 s interval to ensure that the data were long enough for the maximum dispersion time delay. In addition, 10 s of data that do not contain mock FRBs are added to the beginning and ending of the file to ensure that the mock FRB data are searched by HEIMDALL. The distributions of the parameters for the
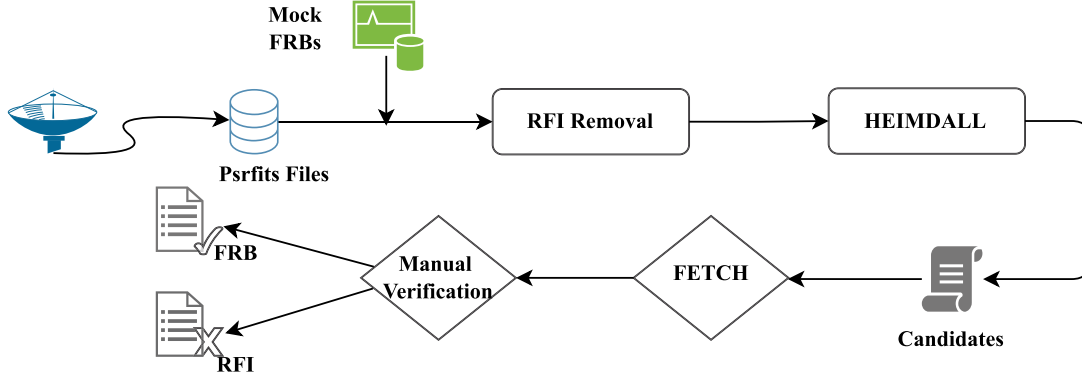
Figure 2. Flow diagram for the key stages of FRB search. First, RFI mitigation is executed on the data. Then search is carried out by employing HEIMDALL to generate candidates. We use FETCH to classify the candidates. Finally, the positive candidates are visually inspected by human eyes.

Table 1
The Distributions of the Injected FRB Parameters for Testing our Search Pipeline

Parameter Name	Distribution
S/N	Uniform(6, 50)
Pulse width	Uniform(0.1, 58) ms
DM	Uniform(100, 3000) pc cm^{-3}
Spectral index	Uniform(-3, 3)
Scattering time	Uniform(0.064, 6.4) ms

simulated FRBs shown in Table 1 were referenced from Agarwal et al. (2020b) and adjusted according to our time resolution (64 μs), observation frequency and bandwidth. These mock FRBs have S/Ns ranging from 6 to 50, DM distribution of 100–3000 pc cm^{-3} and pulse width extent of 0.064–58 ms. These mock FRBs also possess spectral characteristics, such as spectral index (-3, 3) and scattering time (0.064, 6.4 ms). These have covered most of the currently detected parameters of FRBs. The profile of the pulse is composed of a Gaussian shape convolved with an exponential tail, where the scattering is added to the pulse shape. The reference frequency we used is 1500 MHz, for both scattering time and spectral index. The S/N is determined by the rms of the time series after zapping the RFI channels. Before injection, Gaussian noise was added to the profile data and convolved with boxcar width from 0 to 69 ms. In the convolution process, the maximum S/N is used as the injected S/N, and the corresponding width is regarded as the injected width. About 350 mock FRBs with a width greater than the maximum width of 65.536 ms are excluded in this test.

Our injection code is based on FRB Faker[9] and Furby[10], and we injected all mock FRBs before RFI cleaning. Figure 3

---
[9] https://gitlab.com/houben.ljm/frb-faker
[10] https://github.com/vivgastro/Furby

depicts the distributions of S/N, DM and pulse width of the injection FRBs. The broadening effect of intra-channel dispersion and scattering affect the width of the mock FRBs, resulting in a lack of sources with narrow widths in the injections. After injection, the data were searched by employing the pipeline described above with DM from 90 to 3010 pc cm^{-3}, boxcar max of 1024 (65.536 ms) and S/N threshold of 6. For every injected mock FRB, if the DM of the candidate detected by HEIMDALL is within the range of ±100 pc cm^{-3} of the injected DM and the time of the candidate is within the range of 200 ms of the injected time, the mock FRB is considered as detected by HEIMDALL. To prevent too many false positive candidates near 100 pc cm^{-3}, the range of DM was limited to ±50 pc cm^{-3} when the injected DM was below 500 pc cm^{-3}. The candidates produced by HEIMDALL were then passed to the models a and b of FETCH, and if the probability of a candidate is $\geqslant0.6$, it was counted as a detection by FETCH.

3.2. Results of Injected Mock FRB Search

For all mock FRBs that are injected into the data, HEIMDALL detected 92% of them. Furthermore, both model a and model b of FETCH correctly classified about 95% of those candidates detected by HEIMDALL. The number of injections missed by HEIMDALL is plotted in Figure 4 as a percentage of total injected number against the injected S/N, DM and width. HEIMDALL tends to miss the mock FRBs with low S/N, and about 55% of the mock FRBs with low S/N (<7) were missed by our pipeline and the miss percentage increases rapidly when the S/N is lower than 15. The recovered fraction remains greater than 90% for injected S/N above 15. Although our RFI environment is not very good, the performance of HEIMDALL remains good for mock FRBs with high S/N. Assuming that all parameters of the FRBs fall within the general range, the detection rate for S/N between 10 and 15 is still acceptable ($\gtrsim80\%$).
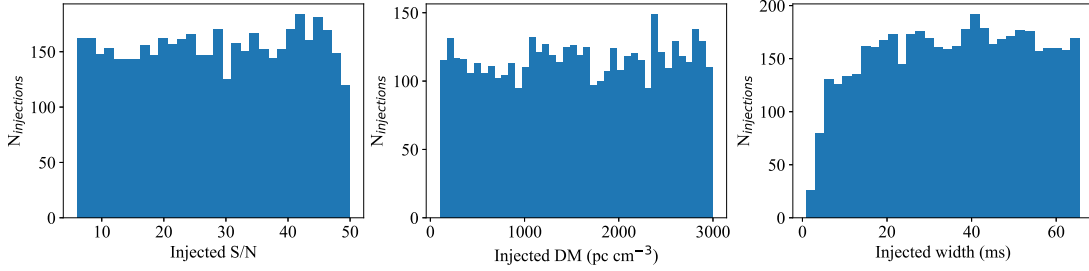
Figure 3. The histograms of the injected mock FRB parameters. From left to right are injected S/N, injected DM and injected width, respectively.
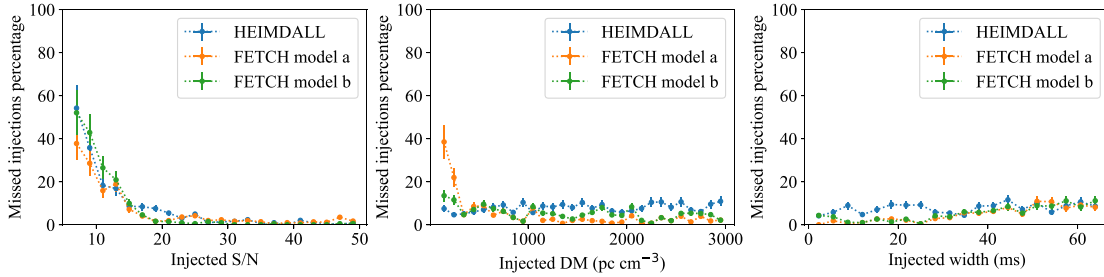

Figure 4. The missed injection percentage by HEIMDALL and FETCH models a and b as a function of the injected S/N, injected DM and injected width with 20% error.
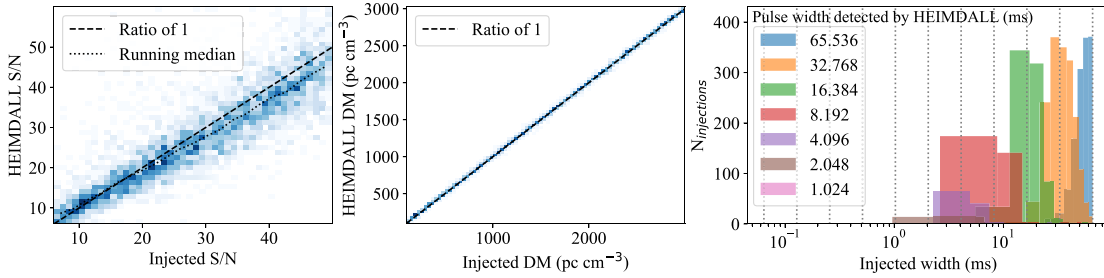

Figure 5. The left and middle plots feature the density distribution of the injected S/N (DM) and the corresponding HEIMDALL detected S/N (DM), respectively. The black dashed line indicates the ratio of 1, and the black dotted line is the running median of the distribution with bin size of 2 S/N unit. The color intensity in the blocks represents the intensity of the density distribution, with darker color signifying higher intensity. The plot on the right is the histogram of injected pulse width for a given boxcar and the vertical dashed line is the width of the boxcar tried by HEIMDALL. The different colored legends represent the widths obtained by HEIMDALL.

Figure 4 also plots the missed percentage of candidates detected by HEIMDALL for models a and b in FETCH. The missed percentages from both models are close to each other and both have a similar trend to HEIMDALL for injected S/N. The missed percentage shows a sign of increasing with the broadening of the pulse width. The increase in the missed percentage of FETCH at low S/N, low DM and high pulse width may be due to the RFI or the RFI mitigation method that we used. The performance of model a is better than model b at low S/N. However, a warning result is that the missed percentage of model a increases rapidly for lower $DM < 300 \, \mathrm{pc \, cm^{-3}}$, probably due to the change of F–T and D–T images caused by zero-DM filtering. Generally, the

FETCH models still have good performance although they are not trained on our real data.

Figure 5 features the comparison of S/N, DM and pulse width values recovered by HEIMDALL with the corresponding injected values, and the histograms of injected width of the mock FRBs detected in a given boxcar trial. After modifying the method of S/N calculation in HEIMDALL, the detected S/N is still lower than the injected S/N. The nearly 5% decrease may come from the mismatch between the simulated FRB width (and DM) and the closest trial width (and DM) searched by HEIMDALL. It was noted that residual RFI usually makes some mock FRBs be detected with lower S/N. However, for heavily contaminated data, the rms of the time series will
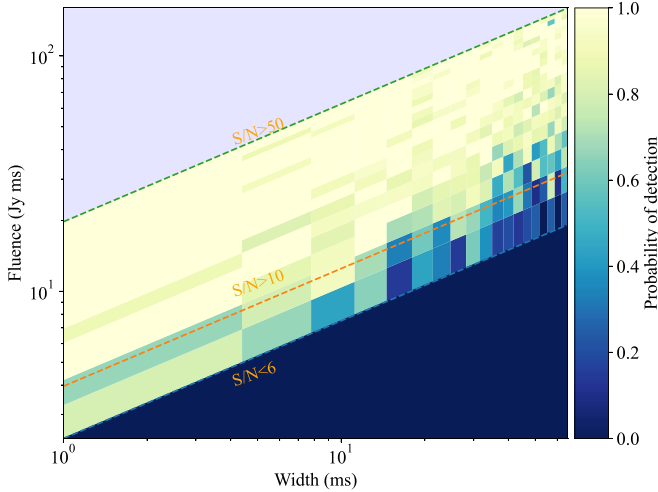
Figure 6. The completeness of our survey for FRBs as a function of their fluences and pulse widths. Green, orange and blue dashed lines indicate constant S/N of 50, 10 and 6, respectively.

reduce after RFI removal, which leads to some recovered S/N being significantly greater than the injected S/N. The DM is recovered well by HEIMDALL and there is only a small offset from the injected value between 100 and 3000 pc cm^{-3}. After adapting HEIMDALL, the distribution of each pulse width does not show significant scattering and long tails.

Figure 6 shows the completeness of our survey for FRBs as a function of their fluences and injected pulse widths. The S/N of 6 is the threshold of HEIMDALL searching and the S/N of 50 is the maximum value of injected FRBs that we simulated. The figure reveals that our pipeline can recover well the FRBs with S/N greater than 15, and an acceptable recovered fraction for those with S/N of 10–15 and pulse width less than 20 ms. It is appropriate to set the S/N threshold to 10 for searching FRBs with consideration of the RFI environment.

3.3. Real Observation Data Testing

In order to test the performance of the pipeline on a real observation, we observed an RRAT source PSR J1819−1458 which has DM of 196 pc cm^{-3} and the burst occurred occasionally with flux greater than the sensitivity of NSRT-26 m. The observations covered two epochs, which included 3.2 hr of epoch 1 (MJD 59,380) and 4 hr of epoch 2 (MJD 59,383), giving a total of 7.2 hr. We searched the data over a DM range of 100–300 pc cm^{-3} and we detected three single pulses with S/N greater than 6 in epoch 1 but none in epoch 2. Figure 7 displays one of the single pulses that we detected from PSR J1819−1458. The reason for non-detection of any bursts in epoch 2 could be due to the decrease of the source flux density or the source being in its quiet phase. Search tests on both simulated data and real observing data demonstrated that our pipeline can search single pulses from FRBs or RRATs.
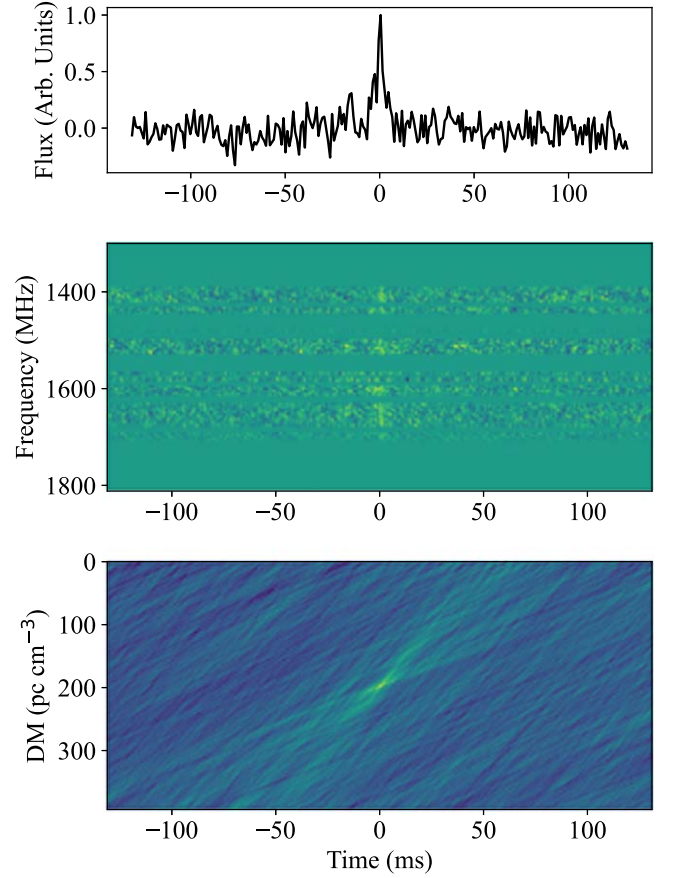

Figure 7. One of the single pulses detected from PSR J1819−1458.

4. Preliminary Search Results of FRB 20201124A

The raw data from FRB 20201124A were converted from full polarization to total intensity by summing AA and BB. For each observation epoch, using the above described pipeline, we searched the data with DM ranging from 350 to 450 pc cm^{-3} and S/N threshold of 6.

Our search pipeline generated more than 6.7×10^5 candidates. Figure 8 shows the distribution of their S/Ns and DMs. The S/Ns of most candidates are between 6 and 20. Due to the residual RFI in the data, some candidates have higher S/N, with 430 candidates having an S/N greater than 50. Candidates with S/N greater than 100 were discarded after visual inspections. For all candidates, model a and model b of FETCH give probabilities of FRBs, which are affirmed in Figure 8. As a result, model a and model b classified 2.05% and 0.43% of all candidates as FRBs with probabilities ⩾0.6, respectively. It is obvious that most of the probabilities are less than 0.6, and model a classified a higher proportion of candidates as FRBs than model b.

To prevent single-pulse candidates from being incorrectly labeled by the classifier, we visually inspected all candidates
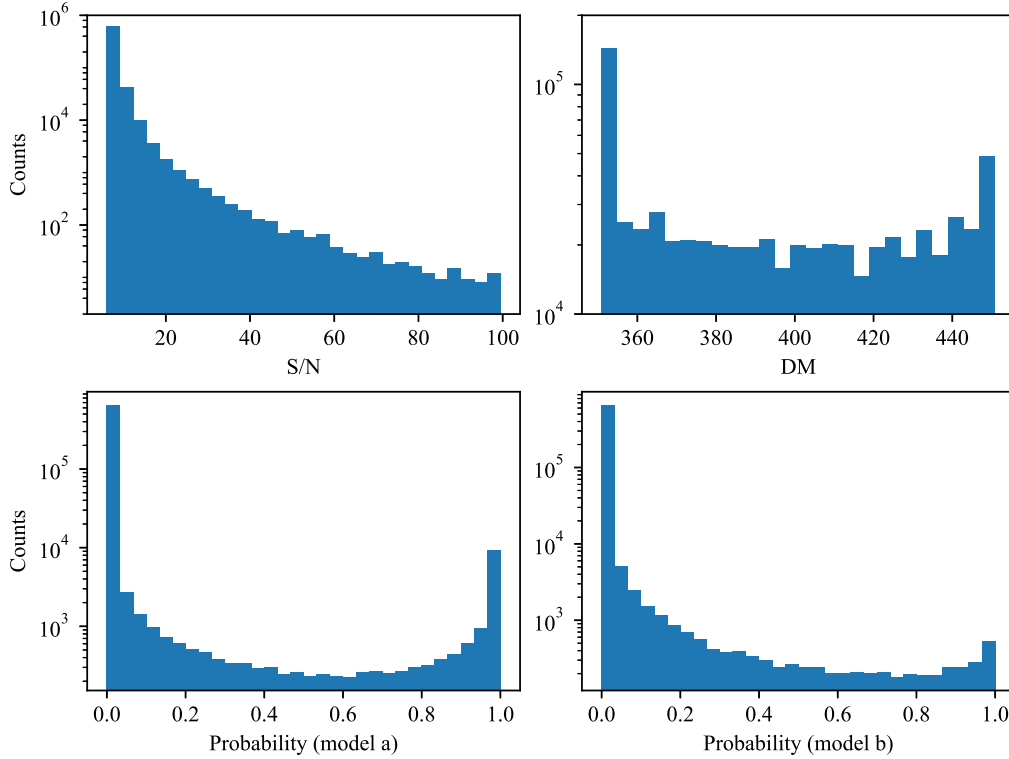
Figure 8. The distributions of S/N and DM for single-pulse candidates are shown in the upper row, and the classification probabilities of the candidates are featured in the lower row.

with a classification probability greater than 0.4 (a total of 1.96×10^4 candidates). In addition, all candidates with S/N > 7 and with DM in the range 400–420 pc cm^{-3} (in the amount of 2.58×10^4) were also plotted and visually inspected. We did not detect single pulse bursts consistent with the DM of FRB 20201124A, nor did we detect any other pulses with astronomical characteristics. The FRB 20201124A was abruptly quenched on 2021 May 29. FAST did not detect any individual pulses during the next 16 days of observation (Xu et al. 2021b). No detection of bursts was reported between June and August 2021, but it was re-detected in 2021 September 21, after which it entered a new active period (Main et al. 2021).

Many bursts of FRB 20201124A exhibit a limited bandwidth characteristic, which can lead to non-detection if the spectrum of the burst is not within our bandwidth. It was reported that the scintillation bandwidth (ν_s) of FRB 20201124A could be modeled with a power law $\nu_s = a\nu^\gamma$, where ν is the observing frequency, and a best-fitting index of $\gamma = 3.5 \pm 0.1$ (Main et al. 2022). The scintillation bandwidth extrapolated to 1.56 GHz is 2.3 ± 0.5 MHz, which is narrower in terms of spectrum than the emission of FRB 20201124A. Therefore, we could exclude the scintillation as the cause of the FRB 20201124A not being

detected. It is likely that FRB 20201124A displays an enriched burst activity phase, and observations presented here were not coincident with such radio-loud windows (Xu et al. 2021b). The lack of detection could indicate a quiescent state, as mentioned by Lanman et al. (2022) and Xu et al. (2021b).

5. Discussion and Conclusions

This article presented the targeted FRB search experiments using the NSRT-26 m, with descriptions of hardware, software and the pipeline. We calculated the minimum detectable fluence as 4 Jy ms. The search pipeline includes mock FRB injections, RFI mitigation, burst search and candidate classification. To study the efficiencies of our pipeline, 5000 mock FRBs were injected into the data and searched by our pipeline. The recovery fraction is related to S/N, DM and pulse width. The results of searching 5000 mock FRBs affirm that our pipeline can recover almost all the ($\gtrsim$90%) injected mock FRBs with S/N > 15. The recovery fraction is still acceptable, $\gtrsim$80%, for those with S/N between 10 and 15. We also test our pipeline using real observation data of RRAT source PSR J1819−1458, which demonstrate that our pipeline can search single pulses from the transient source.

We observed FRB 20201124A with a total exposure time of 104.5 hr, between 2021 June 2 and 2021 July 20, with the result of non-detection. The flux densities of FRB 20201124A are reported to range from 0.005 to 11.5 Jy (Xu et al. 2021b), meaning that only the very bright flashes could be captured by the NSRT-26 m. In addition, this source switches between the energetic phase and inactive phase. It is extinguished from 2021 May 29 to 2021 September 20 and started new activity cycles on 2021 September 21 and 2022 January 23 (Main et al. 2021; Xu et al. 2021b; Ould-Boukattine et al. 2022). Our non-detection of FRB 20201124A might be due to its inactive phase window or emission below the threshold of the Nanshan telescope.

The NSRT-26 m has a relatively large field of view with beam size of about $0°.5$ at L band, and it has the potential advantage to detect some strong FRBs. The actual sensitivity will be significantly reduced due to RFI and non-Gaussian noise. The changes of pulse parameters such as S/N, DM and width will also affect the detection efficiency of the pipeline (Patel et al. 2018). FRBs will also be missed due to some sub-optimal search algorithms (Keane & Petroff 2015). The NSRT-26 m also carried out a blind search for FRBs in real-time between 2016 and 2020 but no detection was reported (Men et al. 2019; Zhang et al. 2021). In the future, we will further optimize the algorithm and improve the search efficiency of our FRB search pipeline. Regular monitorings on some magnetars and known strong repeating FRBs are also planned.

Acknowledgments

ORCID iDs

Yu-Bin Wang, https://orcid.org/0000-0002-9061-6022

References

Agarwal, D., Aggarwal, K., Burke-Spolaor, S., Lorimer, D. R., & Garver-Daniels, N. 2020a, MNRAS, 497, 1661
Agarwal, D., Lorimer, D. R., Surnis, M. P., et al. 2020b, MNRAS, 497, 352
Bochenek, C. D., Ravi, V., Belov, K. V., et al. 2020, Natur, 587, 59
Campana, S. 2021, ATel, 14523, 1
CHIME/FRB Collaboration, Amiri, M., Andersen, B. C., et al. 2020, Natur, 582, 351
CHIME/FRB Collaboration, Amiri, M., Andersen, B. C., et al. 2021a, ApJS, 257, 59
CHIME/FRB Collaboration, Amiri, M., Bandura, K., et al. 2018, ApJ, 863, 48
CHIME/FRB Collaboration, Campana, S., Campana, S., et al. 2021b, ATel, 14497, 1
Eatough, R. P., Keane, E. F., & Lyne, A. G. 2009, MNRAS, 395, 410
Farah, W., Flynn, C., Bailes, M., et al. 2019, MNRAS, 488, 2989
Farah, W., Pollak, A. W., Siemion, A. P. V., et al. 2021, ATel, 14676, 1
Golpayegani, G., Lorimer, D. R., Ellingson, S. W., et al. 2019, MNRAS, 489, 4001
Gupta, V., Flynn, C., Farah, W., et al. 2021, MNRAS, 501, 2316
Herrmann, W. 2021, ATel, 14556, 1
Hilmarsson, G. H., Spitler, L. G., Main, R. A., & Li, D. Z. 2021, MNRAS, 508, 5354
Keane, E. F., Barr, E. D., Jameson, A., et al. 2018, MNRAS, 473, 116
Keane, E. F., & Petroff, E. 2015, MNRAS, 447, 2852
Kirsten, F., Ould-Boukattine, O. S., Nimmo, K., et al. 2021, ATel, 14605, 1
Kumar, P., Shannon, R. M., Keane, E., Moss, V. A. & Askap-Craft Survey Science Project 2021a, ATel, 14508, 1
Kumar, P., Shannon, R. M., Lower, M. E., et al. 2022, MNRAS, 512, 3400
Kumar, P., Shannon, R. M., Moss, V., Qiu, H., & Bhandari, S. 2021b, ATel, 14502, 1
Lanman, A. E., Andersen, B. C., Chawla, P., et al. 2022, ApJ, 927, 59
Law, C., Tendulkar, S., Clarke, T., Aggarwal, K., & Bethapudy, S. 2021, ATel, 14526, 1
Law, C. J., Bower, G. C., Burke-Spolaor, S., et al. 2018, ApJS, 236, 8
Lorimer, D. R., Bailes, M., McLaughlin, M. A., Narkevic, D. J., & Crawford, F. 2007, Sci, 318, 777
Main, R., Bethapudi, S., & Marthi, V. 2021, ATel, 14933, 1
Main, R. A., Hilmarsson, G. H., Marthi, V. R., et al. 2022, MNRAS, 509, 3172
Marthi, V. R., Bethapudi, S., Main, R. A., et al. 2022, MNRAS, 509, 2209
Men, Y. P., Luo, R., Chen, M. Z., et al. 2019, MNRAS, 488, 3957
Niu, C.-H., Li, D., Luo, R., et al. 2021, ApJL, 909, L8
Ould-Boukattine, O. S., Kirsten, F., Nimmo, K., et al. 2022, ATel, 15190, 1
Patel, C., Agarwal, D., Bhardwaj, M., et al. 2018, ApJ, 869, 181
Spitler, L. G., Scholz, P., Hessels, J. W. T., et al. 2016, Natur, 531, 202
The CHIME/FRB Collaboration, Andersen, B. C., Bandura, K., et al. 2021, arXiv:2107.08463
Wang, N., Manchester, R. N., Zhang, J., et al. 2001, MNRAS, 328, 855
Wayth, R., Brisken, W., Deller, A., et al. 2011, ApJ, 735, 97
Xu, H., Niu, J., Lee, K., et al. 2021a, ATel, 14518, 1
Xu, H., Niu, J. R., Chen, P., et al. 2021b, arXiv:2111.11764
You, S.-P., Wang, P., Yu, X.-H., et al. 2021, RAA, 21, 314
Zhang, C. F., Xu, J. W., Men, Y. P., et al. 2021, MNRAS, 503, 5223
Zhang, H., & Nie, J. 2016, IEEE, ICOACS, 2016, 185
Zhirkov, K., Lipunov, V., Kornilov, V., et al. 2021, ATel, 14532, 1
Zhu, W., Li, D., Luo, R., et al. 2020, ApJL, 895, L6